NASA Technical Memorandum 81460

NOISE SUPPRESSION DUE TO ANNULUS SHAPING OF AN INVERTED-VELOCITY-PROFILE COAXIAL NOZZLE

J. Goodykoontz and U. von Glahn
Lewis Research Center
Cleveland, Ohio

Prepared for the
Ninety-Ninth Meeting of the
Acoustical Society of America
Atlanta, Georgia, April 21-25, 1980

NOISE SUPPRESSION DUE TO ANNULUS SHAPING OF AN INVERTED-VELOCITY-PROFILE COAXIAL NOZZLE

by J. Goodykoontz and U. von Glahn

National Aeronautics and Space Administration
Lewis Research Center
Cleveland, Ohio 44135

E-369

ABSTRACT

Previous studies have shown that an inverted-velocity-profile coaxial nozzle for use with supersonic cruise aircraft produces less jet noise than an equivalent conical nozzle. Furthermore, decreasing the annulus height (increasing radius ratio with constant flow) results in further noise reduction benefits. In the present model-scale study, the annulus shape, that is, height, was varied by an eccentric mounting of the annular nozzle with respect to a conical core nozzle. Acoustic measurements were made in the flyover plane below the narrowest portion of the annulus and at 90° and 180° from this point. The model-scale spectra are scaled up to engine size (1.07 m diameter) and the perceived noise levels for the eccentric and baseline concentric inverted-velocity-profile coaxial nozzles are compared over a range of operating conditions. The implications of the acoustic benefits derived with the eccentric nozzle to practical applications are discussed.

INTRODUCTION

In recent years, several jet noise reduction concepts have evolved in an effort to meet FAR-36 noise goals for supersonic cruise aircraft. Two concepts are of particular interest; namely, the inverted-velocity-profile (IVP) coaxial/coannular nozzle (refs. 1 to 3) and the shielding of two parallel jets (ref. 4). Experimental data obtained with IVP coaxial/coannular nozzles indicate that jet noise suppression increases with a decreasing radius ratio of the outer high velocity stream. Also, jet-to-jet shielding studies indicate that noise reductions can be achieved when the shielding jet stream is smaller in cross-sectional flow area than that of the primary stream. In such a configuration, the axial jet velocity of the shielding stream decays more quickly than that of primary stream because the decay distance is a function of the nozzle geometry; in this case, the nozzle diameter.

From the preceding considerations, a two-stream IVP nozzle concept was evolved in which nozzle shaping through asymmetrical exhaust nozzle flow passages conceivably could provide additional acoustic benefits over that of a symmetric baseline IVP nozzle. (The latter IVP nozzle would

already be more quiet than a reference conical nozzle.) In the present study, simple nozzle shaping for noise reduction was obtained by modifying an existing concentric coaxial nozzle used in previous acoustic studies (refs. 5 and 6). The nozzle was modified such as to provide an eccentric outer stream annulus, while maintaining approximately the same through-flow as that for the original concentric baseline nozzle. This alteration provided a narrow annulus at one point of the outer nozzle and a wide annulus at 180° or opposite this narrowest point, with a varying annulus width between these two points (fig. 1). The outer stream jet velocity was constant around the circumference of the eccentric annulus at the exhaust plane. As a consequence of the varying circumferential velocity decay around the annulus, a skewed velocity profile should exist in the downstream portion of the exhaust plume, with maximum and minimum velocities in the outer stream corresponding to the widest and narrowest portions of the eccentric annulus. Peak jet noise reductions would be expected to result in a direction below the minimum outer stream annulus width, which in an aircraft application would be the flyover plane. It should be noted that with a conventional bypass nozzle (core velocity greater than bypass velocity), suppression is obtained with the wide portion of the outer stream in the flyover plane (ref. 7) in contrast to the present configuration with which suppression is obtained with the narrow portion of the annulus in the flyover plane. In a practical case, sideline noise reductions are of equal or greater importance compared with the flyover values. The present nozzle concept has less noise reduction as the circumferential angle increases from the flyover position because the outer stream annulus width increases with increasing circumferential angle. Practical applications in which the annulus height would be shaped and be maintained at a constant narrow width for 80° to 120° from the flyover plane are discussed in the paper.

This paper then presents the results of an exploratory experimental program to determine the noise generating characteristics of an inverted-velocity-profile eccentric coaxial nozzle over a range of flow conditions. The results are compared with those for a concentric baseline IVP coaxial nozzle (refs. 5 and 6). Nominal temperatures ranged from 280 to 1100 K with nozzle pressure ratios ranging from 1.8 to 3.0 for the outer stream and 1.6 to 2.2 for the inner stream.

APPARATUS AND PROCEDURE

Facility

A photograph of the flow facility is shown in figure 2. A common source of unheated laboratory air was used to supply flow for two parallel flow lines; one line for the inner nozzle and the other for the outer nozzle. Each flow line had its own air and fuel flow control and flow measuring systems. The air in each line was heated by jet engine

combustors. Mufflers in each line attenuated flow control valve noise and internal combustion noise. The system was designed to give maximum nozzle exhaust temperatures of 1100 K and nozzle pressure ratios up to 3.0 in both the inner and outer stream flow lines.

Acoustic. - Microphones were placed at a constant 5.0 meters distance from and parallel to the nozzle axis, as shown in figure 3. The centerline microphone array consisted of 0.635 cm condenser microphones with the metal protective grids removed to improve the acoustic performance at high frequencies. The ground-plane of the test area was composed of asphalt interspersed with patches of concrete and covered with 15.25 cm thick foam rubber blankets.

Jet plume. - Jet exhaust plume temperature/pressure surveys were made with a probe capable of traversing in the axial direction as well as horizontally and vertically, as illustrated in figure 4. Details of the probe are given in reference 6. This probe was calibrated in a wind tunnel at subsonic and supersonic speeds. Total temperature, total pressure and static pressure were measured. The plume survey apparatus was removed from the test site during the acoustic tests.

Nozzles

Two coaxial nozzle configurations were used in the experimental program; one with a concentric, coplanar exit, and one with an eccentric coplanar exit. Pertinent dimensions of the nozzles are given in figure 5. The area ratio of the nozzle was 1.4 and is defined as the ratio of the outer nozzle flow area to the inner nozzle flow area. The diameters shown in the figure are inside diameters of the respective nozzles. Photographs of the concentric and eccentric coplanar nozzles are shown in figure 6. The outer wall of the inner nozzle was coated with a high-temperature ceramic material to minimize heat transfer between the two streams during coplanar operation. The interior of the upstream portion of the inner nozzle line was also lined with insulating material.

Procedure

Steady-state conditions were attained for each test before the data were recorded. Upstream total temperatures and total pressures for both streams were then automatically recorded, as were the flow-field or acoustic data.

Aerodynamic. - For the jet plume surveys, probe position, total temperature, total pressure, and static pressure were automatically recorded.

Plume measurements were made in a plane passing through the minimum and maximum annulus height points. For each point, flow-field properties were calculated from the measured data. The measured pressures (total and static) were corrected for probe bow-shock effects, when necessary. From these pressures, the local Mach numbers were then calculated. Total temperature measurements were corrected for thermocouple radiation losses. Static temperatures were then computed from the Mach numbers and corrected total temperatures, and the local velocities were then calculated.

Acoustic. - For the acoustic tests, the noise signals from the microphone were sequentially analyzed on-line, and 1/3-octave-band sound pressure levels were digitally recorded on magnetic tape for further processing. Acoustic measurements were made in a plane passing through the minimum and maximum annulus height points, as well as at 90° to this plane by rotating the outer nozzle about its axis.

In order to obtain full-scale perceived noise levels, PNL, the model-scale noise spectra were scaled for size (1.07 m equivalent nozzle exhaust diameter), distance, and atmospheric attenuation and frequency-shifted using the Strouhal relationship. From such full-scale spectra PNL values were computed for a standard day (288 K at 70% R.H.) at a flyover height of 338 m.

From plots of full-scale PNL values as a function of distance along the flight path, a flyover relative noise level (FRNL) was computed as described in appendix A of reference 8. The term "relative" is used herein since the conventional definition of effective perceived noise level (EPNL) includes forward flight effects, whereas the present data are for static conditions. The omission of flight effects, however, does not significantly affect the present flyover relative noise level comparisons between the various configurations. Comparisons of relative flyover noise levels of the concentric and eccentric nozzles were then made.

Summary of Flow Conditions

The flow conditions used in the present acoustic study are summarized in the following table.

ECCENTRIC NOZZLE FLOW CONDITIONS

Operational mode	PR_o	T_o, K	V_o, m/s	PR_i	T_i, K	V_i, m/s	V_i/V_o
All subsonic	1.8	1089	587	1.6	288	280	0.48
	1.8*	1089*	585*	1.6*	811*	463*	.79*
Supersonic V_i, Subsonic V_o	1.8	1089	578	2.2	288	341	.59
Subsonic V_i, Supersonic V_o	2.2	1089	660	1.6	288	278	.42
	2.2*	1089*	669*	1.6*	811*	471*	.70*
	3.0	1089	766	1.6	288	272	.36
	3.0*	1089*	780*	1.6*	811*	458*	.59*
All supersonic	3.0	1089	768	2.2	288	341	.44
	3.0	1089	767	2.2	811	580	.76

The conditions marked with an asterisk were those for which plume surveys were obtained. Similar flow conditions were used with the concentric nozzle.

JET PLUME SURVEYS

The jet plume of the eccentric nozzle was surveyed in the flyover plane at five axial downstream stations. From the measured pressure and temperature data, local stream Mach numbers were calculated and are shown in figures 7 and 8 as a function of radial position. Two cases are shown: (1) both streams subsonic (fig. 7) and (2) the outer stream supersonic with the inner stream subsonic (fig. 8). Also shown, for comparison, are similar Mach number profiles for the concentric nozzle. The Mach number profiles clearly show the rapid decay of the narrow-gap-annulus velocity with axial downstream distance and the persistence of the wide-gap-annulus velocity with axial downstream distance. Also apparent is the asymmetry of the Mach number profile for the eccentric nozzle at large axial downstream distances (X/D_i = 11). In general, the velocity (Mach number) decay trends of thejet plume was similar for the flow conditions indicated in figures 7 and 8 as well as those not shown. Information such as that shown in figures 7 and 8 should prove useful for future analytical studies of noise source alteration due to jet shaping.

MODEL-SCALE SPECTRAL DATA

Representative measured spectral data in the flyover plane ($\varphi = 0^{\circ}$) for the concentric nozzle obtained at model scale are compared with those for the eccentric nozzle in figure 9. The data shown are for a radiation angle, θ, of 129° and the flow conditions given in the figure. It is apparent that for this radiation angle, a suppression in SPL is obtained with the eccentric nozzle for model scale frequencies greater than about 1650 hertz. For frequencies below 1650 hertz, the spectra for the two nozzles are essentially the same; that is, no noise suppression is obtained with the eccentric nozzle. Also shown on the abscissa in the figure is a second scale that identifies the frequencies and sound pressure level region associated with a full-size supersonic cruise aircraft engine having total exhaust nozzle area of 0.9 m^2 (1.07 m equivalent diameter). Hereinafter, all the acoustic data will be scaled to and presented for this engine size.

ENGINE-SIZE SPECTRA

In the following section, representative spectra for several conceptual engine cycles are presented for both the eccentric and concentric nozzles at engine size. The engine cycle concepts consist of: (1) both streams subsonic, (2) inner stream supersonic and outer stream subsonic, (3) inner stream subsonic, outer stream supersonic, and (4) both streams supersonic. In all cases, by adjustment of stream temperatures, the outer stream velocity is greater than that of the inner stream. Concepts 3 and 4 represent variable stream engine cycles currently being considered for supersonic cruise aircraft.

Flyover Plane ($\varphi = 0^{\circ}$)

For each of the preceding cycle concepts, representative engine-size spectra will be shown for the forward quadrant ($\theta = 46^{\circ}$), nearly overhead flyover ($\theta = 95^{\circ}$), and rear quadrant ($\theta = 129^{\circ}$).

Forward quadrant ($\theta = 46^{\circ}$). - The spectra for both the eccentric and concentric nozzles are shown in figure 10 for the four engine cycle concepts. In general, no suppression is achieved by the eccentric nozzle in the forward quadrant in the flyover plane. An exception was noted when the inner stream was supersonic and the outer stream subsonic (fig. 10(b)). For this case, low frequency mixing and shock noise were less for the eccentric nozzle than those for the concentric nozzle. Although some additional noise can be observed at low frequencies with the eccentric nozzle for some cases, this is more probably associated with ground reflection variations in the test arena.

Flyover ($\vartheta = 95^{\circ}$). - Representative spectra for the four cycle concepts are shown in figure 11 for a nearly overhead flyover location. In general, the spectra for the eccentric and concentric nozzles are the same. Except for the previously noted case for $\vartheta = 46^{\circ}$, any apparent deviation of the data appear to be within data repeatability and/or associated with ground reflections in the test arena. Consequently, the eccentric nozzle shows no acoustic benefits over the concentric nozzle for the overhead location.

Rear quadrant ($\vartheta = 129^{\circ}$). - Representative spectra for the illustrative engine cycles are shown in figure 12 near the peak noise angle in the flyover plane. In all cases, the eccentric nozzle provided noise supression compared with noise produced by the concentric nozzle. In general, the spectral reductions occurred at engine-size frequencies greater than 250 hertz.

Sideline ($\varphi = 90^{\circ}$) and Overhead ($\varphi = 180^{\circ}$)

In general, the spectra for the eccentric nozzle at φ of 90° and 180° (see fig. 1) were the same as those for the concentric nozzle except for slight deviations in the spectra in the lower frequency range for θ of 129° and 139°. At these frequencies, the concentric nozzle, in some cases, had lower SPL values than those for the eccentric nozzle by locally up to 5 dB. These deviations again are believed to be primarily due to variations in ground reflections.

Effect of Cycle Conditions on Spectra

The effect of changing either the inner or outer stream velocity while maintaining the other constant is shown in the next several figures for radiation angles of 115°, 129°, and 148°. The data are shown as an SPL difference between the concentric and eccentric nozzle, $\Delta SPL = SPL_E - SPL_C$, as a function of engine-size frequency.

Constant V_i, variable V_o. - In figures 13 to 15 are shown the variation of ΔSPL with frequency for constant inner stream nominal velocities of 274, 341, and 464 m/s. The outer stream nominal velocity was varied from 578 to 780 m/s, depending on the magnitude of the inner stream velocity.

Significant SPL suppressions were generally obtained in the mid to high frequency ranges for radiation angles equal to and greater than 129°. At low frequencies, usually less than 250 hertz some additional noise appeared to be incurred with the eccentric nozzle. This was significant only at a radiation angle of 129°. It is not known at this time, whether this added noise was due to ground reflection effects or was indeed

attributable to the eccentric nozzle noise signature. Because of the limited data, general trends in the local SPL values with operating conditions cannot be ascertained with any degree of confidence. While certain SPL data indicate frequency and level trends with variations in outer stream velocity, particularly at $\theta = 148^{\circ}$, other data do not. In general, however, changes in the outer stream velocity with a fixed inner stream velocity for the most part do not significantly influence the SPL suppressions attained with the eccentric nozzle.

Constant V_o, variable V_i. - In figures 16 to 18 are shown the variation of ΔSPL with frequency for constant outer stream nominal velocites of 583, 665, and 770 m/s. The inner stream nominal velocity was varied from 272 to 580 m/s depending on the magnitude of the outer stream velocity.

As in the previous discussion, it is apparent that general acoustic trends between the various flow conditions are difficult to establish. It does appear, however, that at $\theta = 129^{\circ}$, the data with a nominal outer stream velocity of 770 m/s (fig. 18(c)) shows a greater SPL suppression at frequencies above 1000 hertz than that at the two lower outer stream velocities. This trend is reversed at $\theta = 148^{\circ}$.

PERCEIVED NOISE LEVELS

From the measured spectra for the concentric and eccentric nozzles, the engine-size perceived noise levels were calculated as a function of distance along the flight path. A representative variation of PNL as a function of distance along the flight path is shown in figure 19. For the specific operating conditions noted on the figure, it is apparent that significant noise reduction is obtained with the eccentric nozzle in the PNL region important for noise certification (i.e., 10 PNdB down from the peak PNL value).

The reduction in PNL obtained by use of the eccentric nozzle is shown in figure 20 for all flow conditions in terms of a $\Delta PNL = PNL_E - PNL_C$ as a function of the distance along the flight path. The data show that the PNL values for the eccentric nozzles are suppressed in the rear quadrant ($\theta > 90^{\circ}$). Maximum suppressions of about 3 to 5 PNdB were obtained at the peak noise angles for the cycle concepts included in the study. Significant PNL suppressions were obtained in the forward quadrant only with a subsonic outer stream and a supersonic inner stream (fig. 20(b)),

FLYOVER RELATIVE NOISE LEVEL

From PNL plots, such as that shown in figure 19, flyover relative noise levels (FRNL) were calculated by the method of reference 8. The change in FRNL values between the concentric and eccentric nozzles for the nine operating modes included herein are shown in the following table by ΔFRNL, where $\Delta FRNL = FRNL_E - FRNL_C$.

SUMMARY OF FLYOVER RELATIVE NOISE LEVELS

Operational mode	V_o, m/s	V_i, m/s	PR_o	PR_i	V_i/V_o	ΔFRNL, EPNdB
All subsonic	587	280	1.8	1.6	0.48	-1.5
	585	463	1.8	1.6	.79	-1.9
Supersonic V_i, Subsonic V_o	578	341	1.8	2.2	.59	-1.9
Subsonic V_i, Supersonic V_o	660	278	2.2	1.6	.42	-1.5
	669	471	2.2	1.6	.70	-2.8
	766	272	3.0	1.6	.36	-1.5
	780	458	3.0	1.6	.59	-2.3
All supersonic	768	341	3.0	2.3	.44	-1.0

As shown in the preceding table, ΔFRNL values of -1 to -2.8 EPNdB are achieved with the eccentric nozzle when compared with the concentric nozzle noise levels. Also shown is that higher ΔFRNL values are obtained with V_i/V_o ratios near 0.7 than with those near 0.4.

The least amount of suppression appears to occur for the case of both streams operating at supersonic pressure ratios. However, the ΔFRNL of -1.0 for this case compared with -1.5 for the operational modes in the same V_i/V_o ratio range may be within the repeatability of the test data.

PRACTICAL APPLICATION CONSIDERATIONS

For purposes of practical application noise suppression is generally desired both in the sideline plane ($\varphi = 65^\circ$) and the flyover plane ($\varphi = 0^\circ$). The eccentric nozzle provides maximum suppression in the flyover plane, with decreasing suppression as φ increases toward 90°.

However, by shaping the annulus with a constant narrow width to $\varphi = 90^{\circ}$, or even greater, sideline suppression should be achievable. By following this procedure, the annulus width must be increased for φ values larger than the φ_{max} for the narrow width annulus. This, in essence, yields an "egg shaped" annulus (fig. 21) for the present nozzle concept.

Consider now nozzle shaping as a concept for plug-type nozzles. Data, not included herein, obtained with the present eccentric nozzle with flow in the annulus only (inner stream flow shutoff), showed noise reductions occurring in the rear quadrant. This is perhaps indicative of what might occur with a single stream plug nozzle. The magnitude of the reductions were similar to those obtained with both streams flowing. The noise reduction was obtained with the narrow portion of the annulus oriented in the flyover plane.

In figure 22 is shown a possible two-stream plug nozzle concept utilizing nozzle shaping to obtain additional noise suppression over the respective baseline configuration based on the preceding discussion and data included herein. The nozzle configuration shown consists of an inverted velocity profile nozzle concept utilizing an inner stream plug nozzle and an outer stream annular nozzle. For this case, both annuli have the narrow portions of the annulus in the flyover and sideline planes.

It is expected that further substantial noise suppression can be achieved with shaped nozzles by incorporating suppressor elements into the design concept. Such nozzle concepts could consider both full outer annulus and/or core stream suppressors, or partial suppressors in the exhaust streams. The application of such suppressors could not only reduce the jet noise but could enhance the usual suppressor noise reduction of the baseline nozzles by advantageously altering the jet plume velocity profile.

CONCLUDING REMARKS

From a brief experimental exploratory study, it has been determined that additional directional noise suppression benefits can be obtained with nozzle shaping compared with those obtained with a baseline nozzle. The noise benefits were obtained with an eccentric coaxial nozzle using inverted velocity profiles applicable to either subsonic and supersonic cruise aircraft. The noise benefits generally were limited directionally to the rear quadrant. Applications of the study to other IVP nozzle concepts indicated potential benefits for coannular plug-type nozzles. Effects of non-coplanar two-stream nozzle arrangements on the potential benefits of nozzle shaping remain to be assessed. Finally, the effect of nozzle shaping on suppressed coplanar mixer nozzles for supersonic cruise aircraft also must be evaluated.

APPENDIX A

SYMBOLS

D	nozzle diameter
EPNL	effective perceived noise level, EPNdB
FRNL	flyover relative noise level, EPNdB
PNL	perceived noise level, PNdB
PR	stream pressure ratio
SPL	1/3-octave-band sound pressure level, dB re 20μ N/m^2
T	stream total temperature
V	stream velocity
X	axial distance
φ	circumferential angle (fig. 1)
θ	radiation angle

Subscripts:

C	concentric
E	eccentric
i	inner stream
o	outer stream

REFERENCES

1. H. Kozlowski and A. B. Packman, "Aerodynamic and Acoustic Tests of Duct-Burning Turbofan Exhaust Nozzles," NASA CR-2628 (1976).

2. P. R. Knott, E. J. Stringas, J. F. Brausch, P. S. Staid, P. H. Heck, and D. Latham, "Acoustic Tests of Duct-Burning Turbofan Jet Noise Simulation," NASA CR-2966 (1978).

3. O. A. Gutierrez, "Aeroacoustic Studies of Coannular Nozzles Suitable for Supersonic Cruise Aircraft Applications," Proceedings of the SCAR Conference, Part 2, NASA CP-001, 1976, pp. 471-490.

4. W. V. Bhat, "Experimental Investigation of Noise Reduction from Two Parallel-Flow Jets," AIAA J., 16, 1160-1167 (1978).

5. J. H. Goodykoontz and J. R. Stone, "Experimental Study of Coaxial Nozzle Noise," AIAA Paper No. 79-631 (Mar. 1975), also NASA TM-79090 (1979).

6. J. R. Stone, J. H. Goodykoontz, and O. A. Gutierrez, "Effects of Geometric and Flow-Field Variables on Inverted-Velocity-Profile Coaxial Jet Noise," AIAA Paper No. 79-635 (Mar. 1979), also NASA TM-79095 (1979).

7. U. von Glahn and J. Goodykoontz, "Noise Suppression Due to Annulus Shaping of a Conventional Coaxial Nozzle," To be presented at the 99th Meeting of the Acoustical Society of America, Atlanta, GA (Apr. 21-25, 1980), also NASA TM-81461 (1980).

8. D. Groesbeck and U. von Glahn, "Assessment at Full Scale of Nozzle/Wing Geometry Effects on OTW Aeroacoustic Characteristics," NASA TM-79168 (1979).

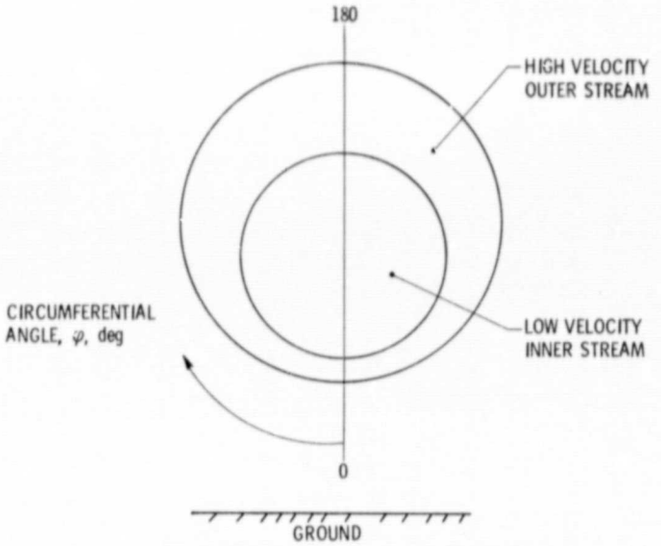

Figure 1. - Eccentric inverted-velocity-profile nozzle.

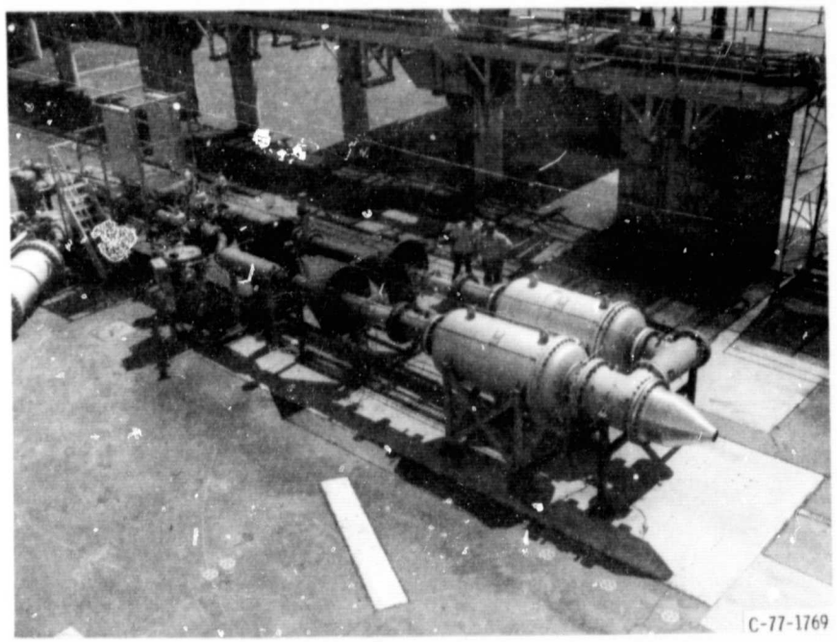

Figure 2. - Coaxial jet flow facility.

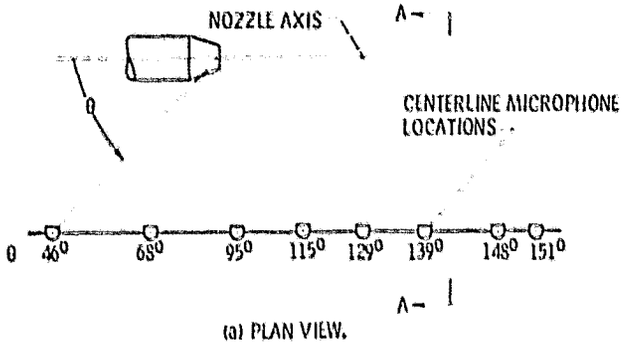

(a) PLAN VIEW.

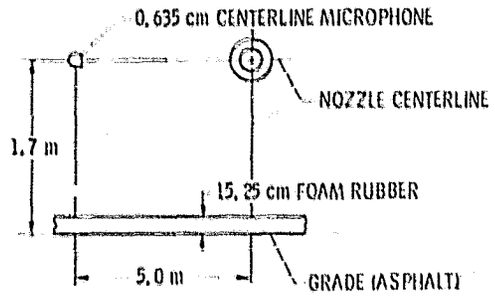

(b) ELEVATION VIEW, VIEW A-A.

Figure 3. - Microphone layout.

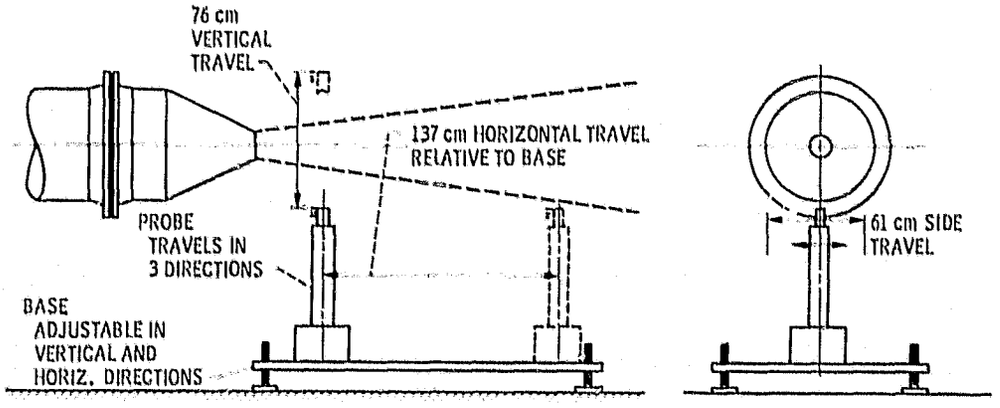

Figure 4. - Jet plume survey arrangement.

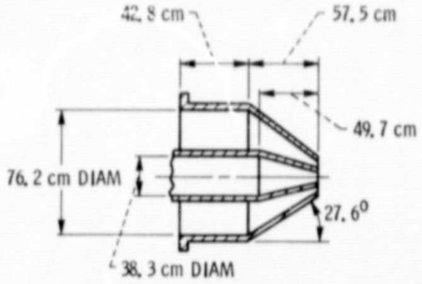

(a) BASIC NOZZLE DIMENSIONS.

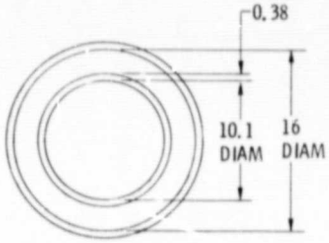

(b) EXIT CROSS-SECTION, CONCENTRIC NOZZLE.

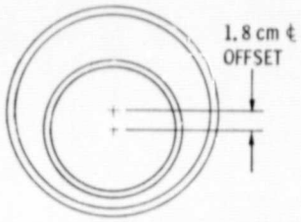

(c) EXIT CROSS SECTION, ECCENTRIC NOZZLE.

Figure 5. - Schematic of coaxial nozzles. All dimensions in centimeters.

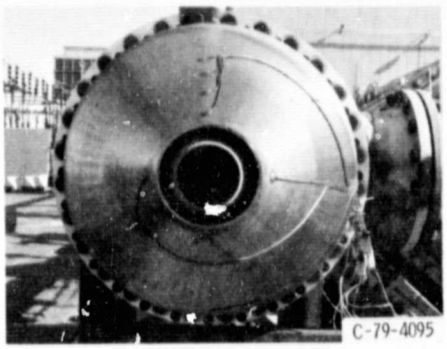

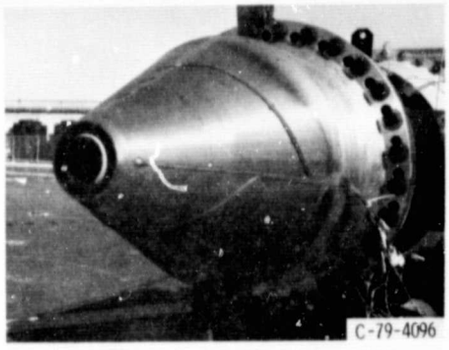

(a) CONCENTRIC NOZZLE.

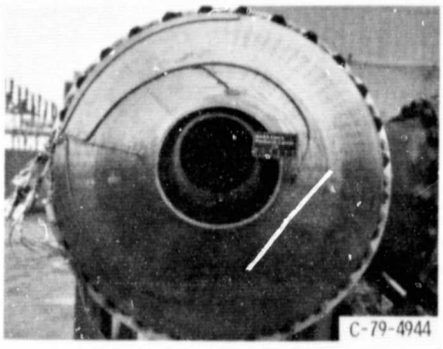

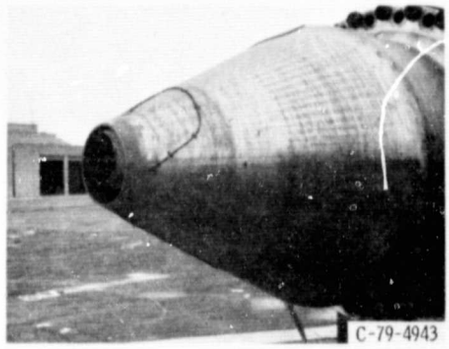

(b) ECCENTRIC NOZZLE.

Figure 6. - Photographs of concentric and eccentric IVP nozzles.

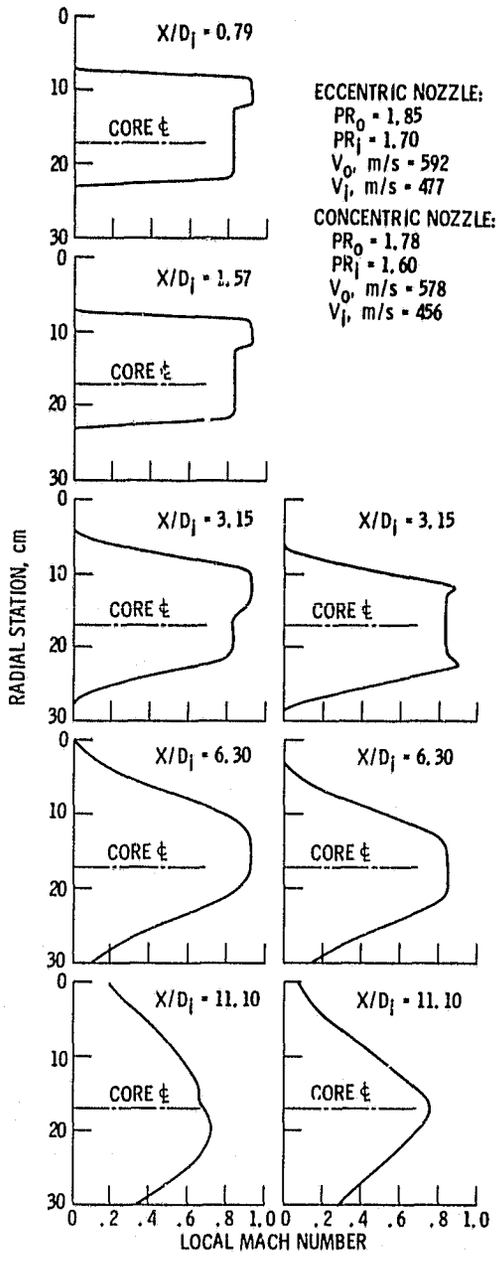

(a) ECCENTRIC NOZZLE. (b) CONCENTRIC NOZZLE.

Figure 7. – Comparison of plume Mach number profiles for eccentric and concentric nozzles at several axial stations – both streams subsonic.

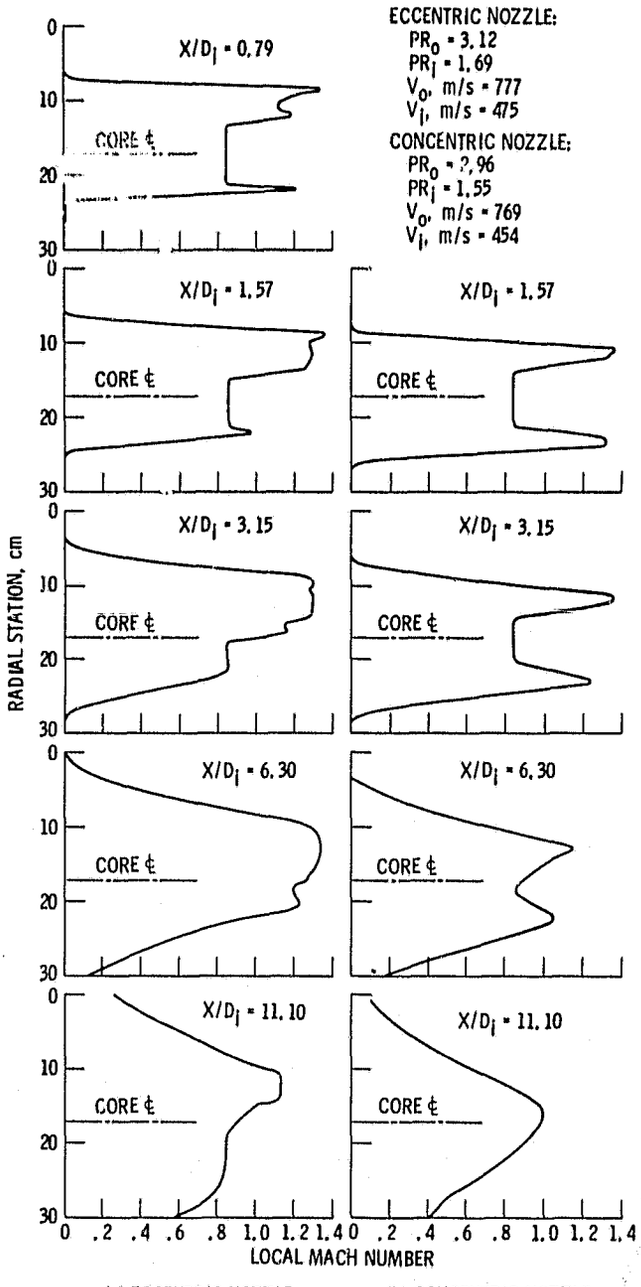

(a) ECCENTRIC NOZZLE. (b) CONCENTRIC NOZZLE.

Figure 8. – Comparison of plume Mach number profiles for eccentric and concentric nozzles at several axial stations – outer stream supersonic, inner stream subsonic.

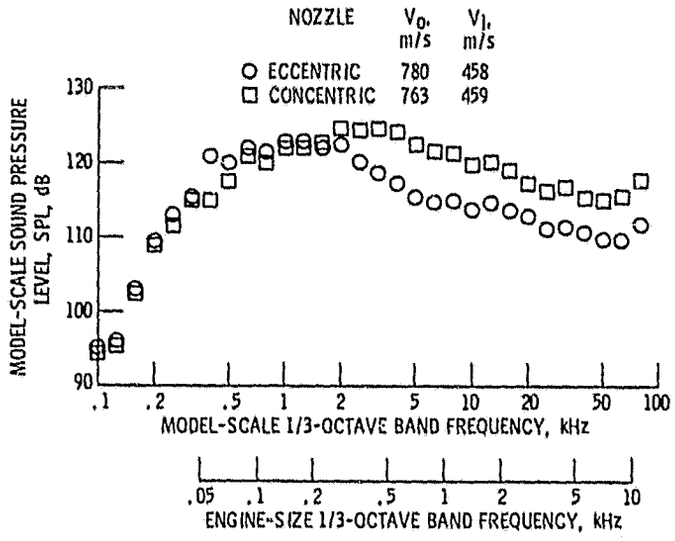

Figure 9. - Illustration of representative model-scale spectra applicable to engine size noise characteristics. Radiation angle, θ, 129°; PR_i, 1.6; PR_o, 3.0; engine/model nozzle scale factor, 6.9; φ, 0°.

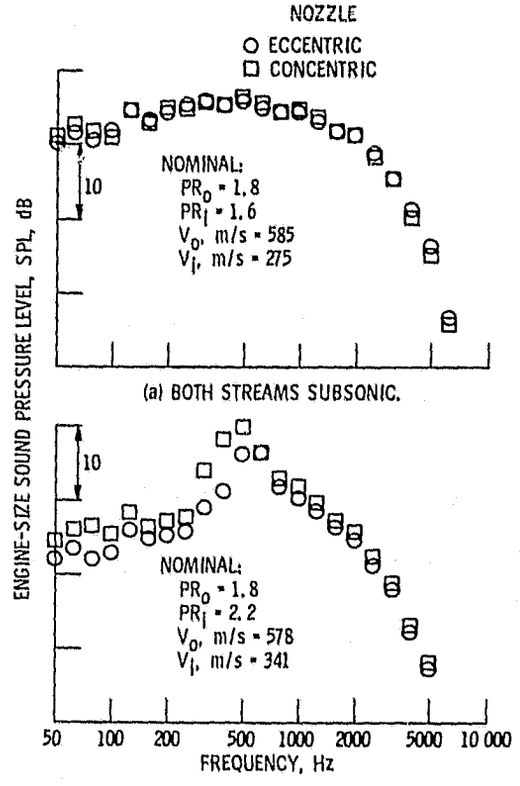

(b) INNER STREAM SUPERSONIC, OUTER STREAM SUBSONIC.

Figure 10. - Representative cycle spectra at 46° radiation angle.

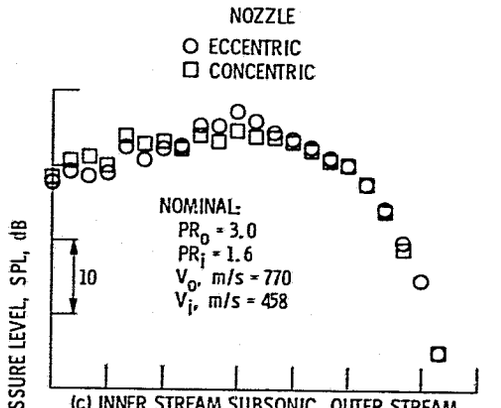

(c) INNER STREAM SUBSONIC, OUTER STREAM SUPERSONIC.

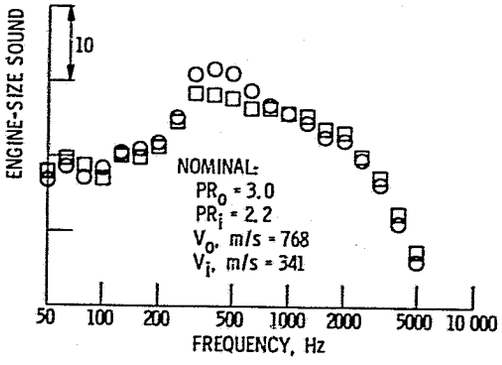

(d) BOTH STREAMS SUPERSONIC.

Figure 10. - Concluded.

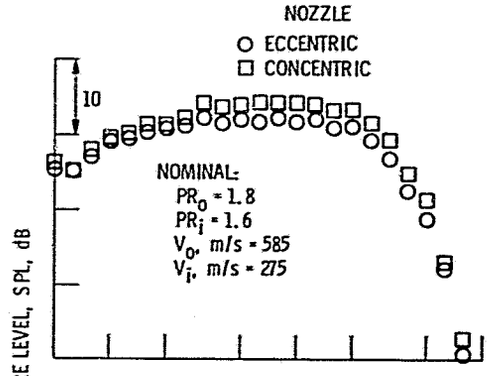

(a) BOTH STREAMS SUBSONIC.

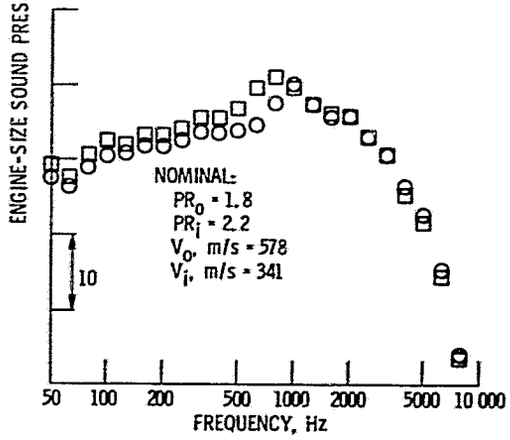

(b) INNER STREAM SUPERSONIC, OUTER STREAM SUBSONIC.

Figure 11. - Representative cycle spectra at 95° radiation angle.

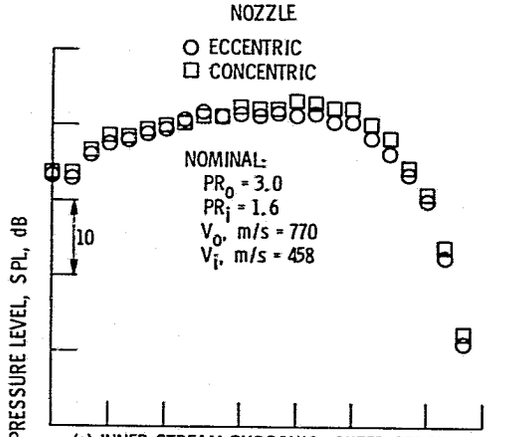

(c) INNER STREAM SUBSONIC, OUTER STREAM SUPERSONIC.

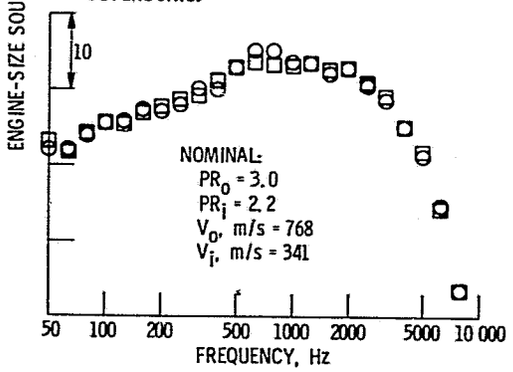

(d) BOTH STREAMS SUPERSONIC.

Figure 11. – Concluded.

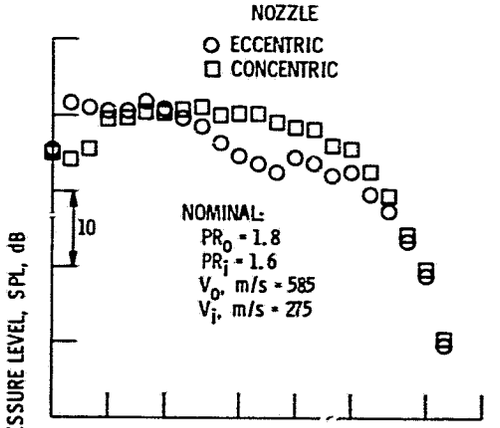

(a) BOTH STREAMS SUBSONIC.

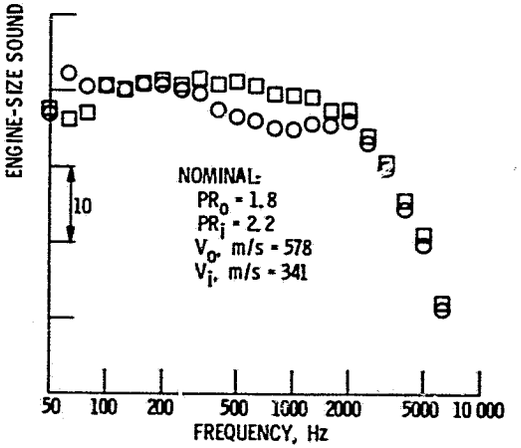

(b) INNER STREAM SUPERSONIC, OUTER STREAM SUBSONIC.

Figure 12. – Representative cycle spectra at 129° radiation angle.

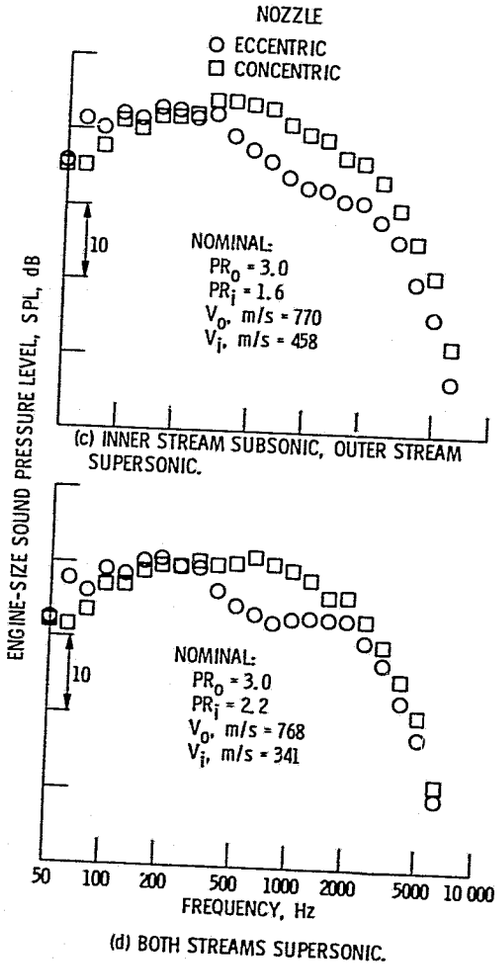

(c) INNER STREAM SUBSONIC, OUTER STREAM SUPERSONIC.

(d) BOTH STREAMS SUPERSONIC.

Figure 12. - Concluded.

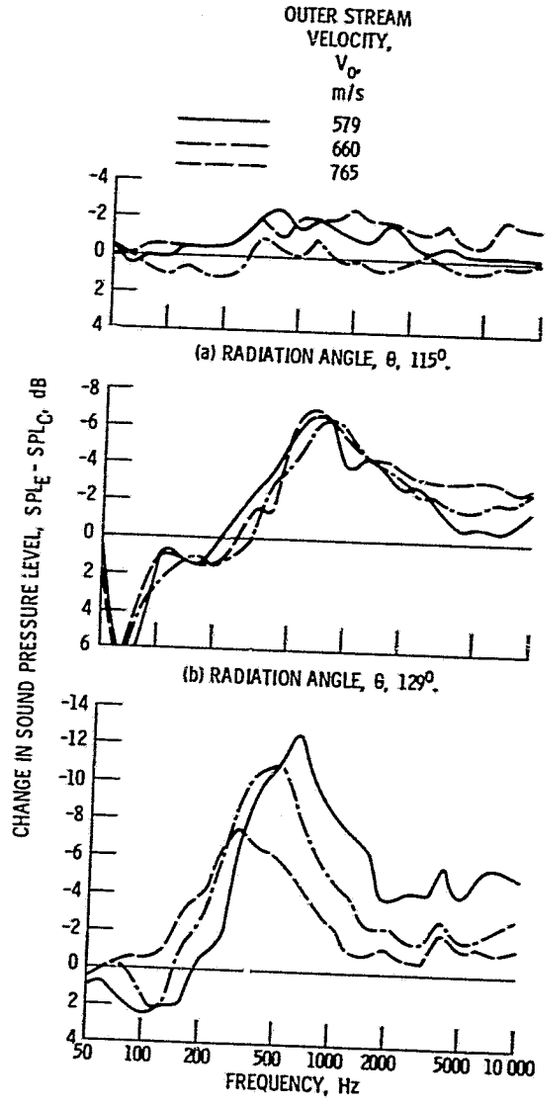

(a) RADIATION ANGLE, θ, 115°.

(b) RADIATION ANGLE, θ, 129°.

(c) RADIATION ANGLE, θ, 148°.

Figure 13. - Variation of rear quadrant $SPL_E - SPL_C$ with constant inner stream nominal velocity, V_i, 274 m/s and various outer stream velocities.

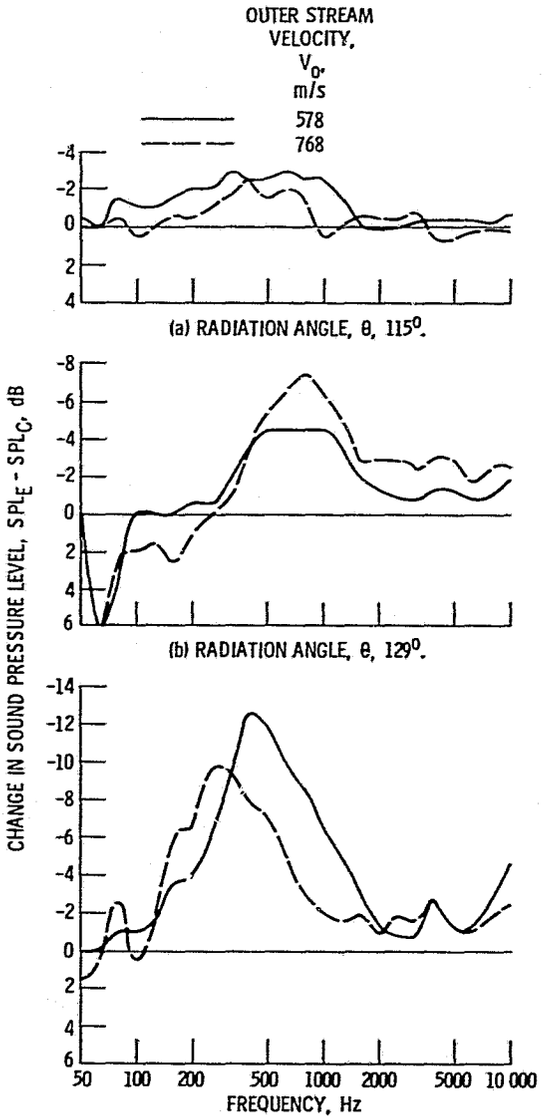

(a) RADIATION ANGLE, θ, 115°.

(b) RADIATION ANGLE, θ, 129°.

(c) RADIATION ANGLE, θ, 148°.

Figure 14. – Variation of rear quadrant $SPL_E - SPL_C$ with constant inner stream nominal velocity, V_i, 341 m/s and various outer stream velocities.

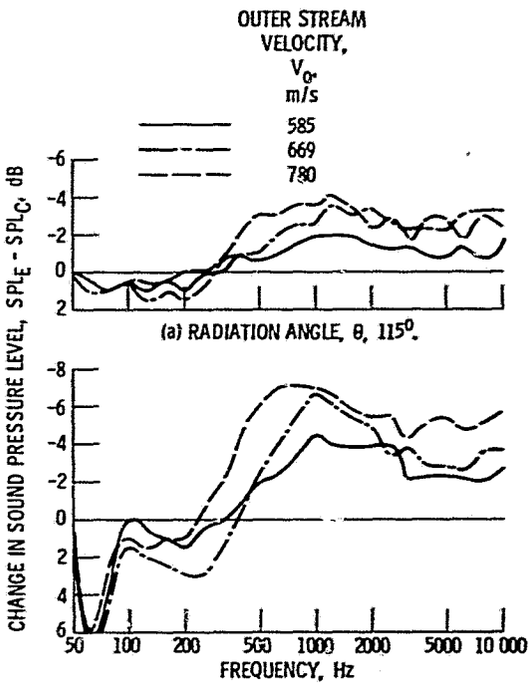

(a) RADIATION ANGLE, θ, 115°.

(b) RADIATION ANGLE, θ, 129°.

Figure 15. – Variation of rear quadrant $SPL_E - SPL_C$ with constant inner stream nominal velocity, V_i, 464 m/s and various outer stream velocities.

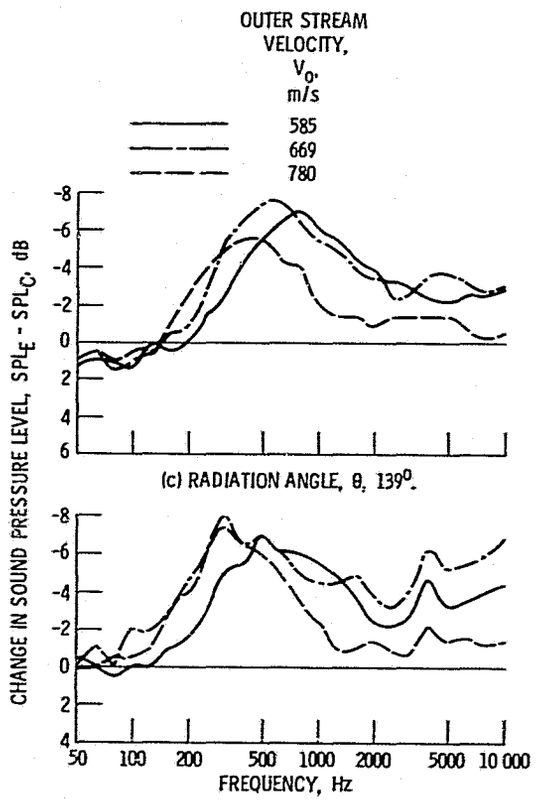

(c) RADIATION ANGLE, θ, 139°.

(d) RADIATION ANGLE, θ, 148°.

Figure 15. - Concluded.

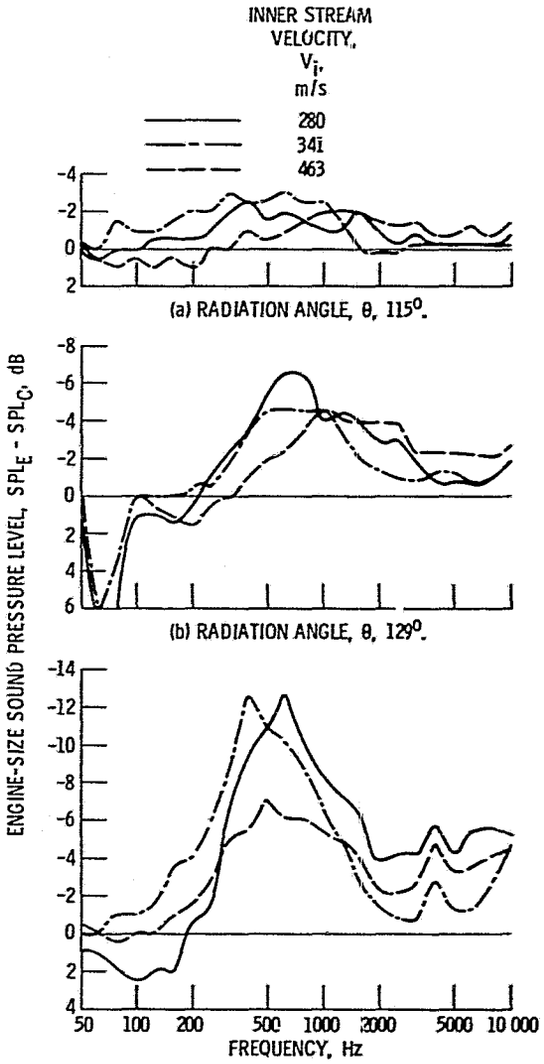

(a) RADIATION ANGLE, θ, 115°.

(b) RADIATION ANGLE, θ, 129°.

(c) RADIATION ANGLE, θ, 148°.

Figure 16. - Variation of rear quadrant $SPL_E - SPL_C$ with constant outer stream nominal velocity, V_o, 583 m/s and various inner stream velocities.

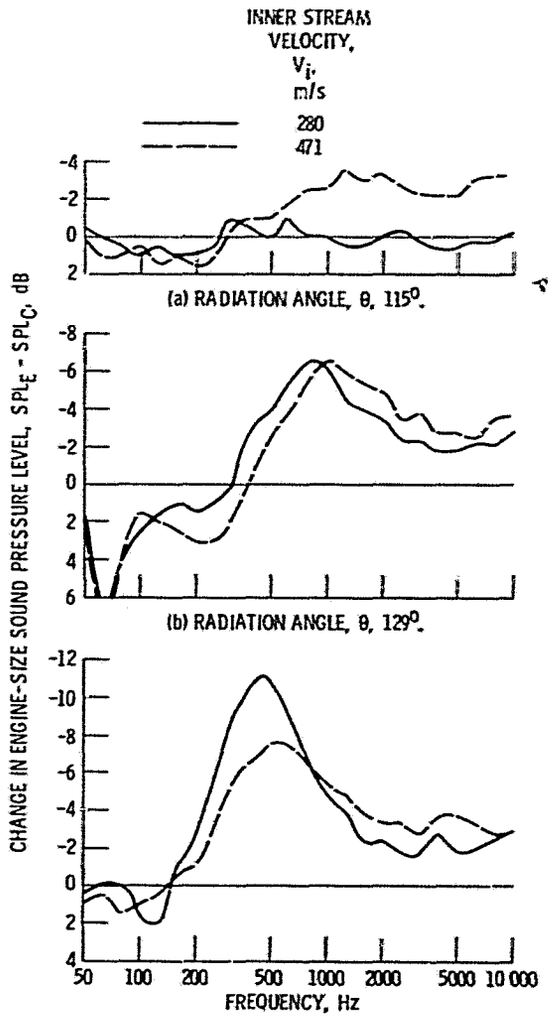

(a) RADIATION ANGLE, θ, 115°.

(b) RADIATION ANGLE, θ, 129°.

(c) RADIATION ANGLE, θ, 148°.

Figure 17. - Variation of rear quadrant $SPL_E - SPL_C$ with constant outer stream nominal velocity, V_o, 665 m/s and various inner stream velocities.

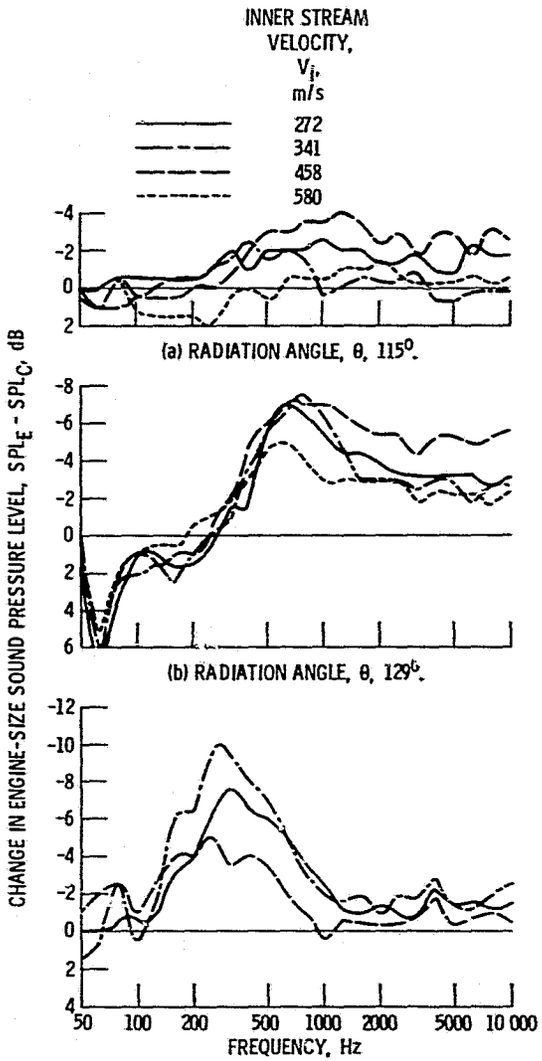

Figure 18. – Variation of rear quadrant $SPL_E - SPL_C$ with constant outer stream nominal velocity, V_o, 770 m/s and various inner stream velocities.

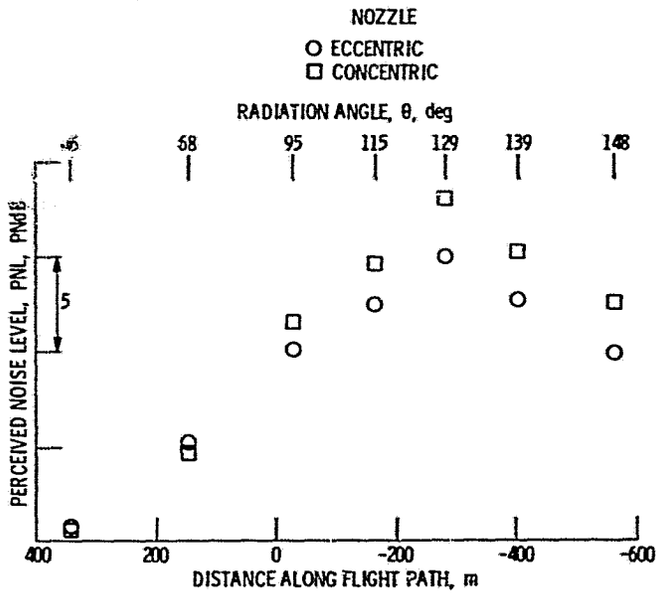

Figure 19. – Representative flyover PNL comparison between eccentric and concentric nozzles. Nominal values of: V_o, 770 m/s; V_i, 458 m/s; PR_o, 3.0; PR_i, 1.6; flyover height, 338 m.

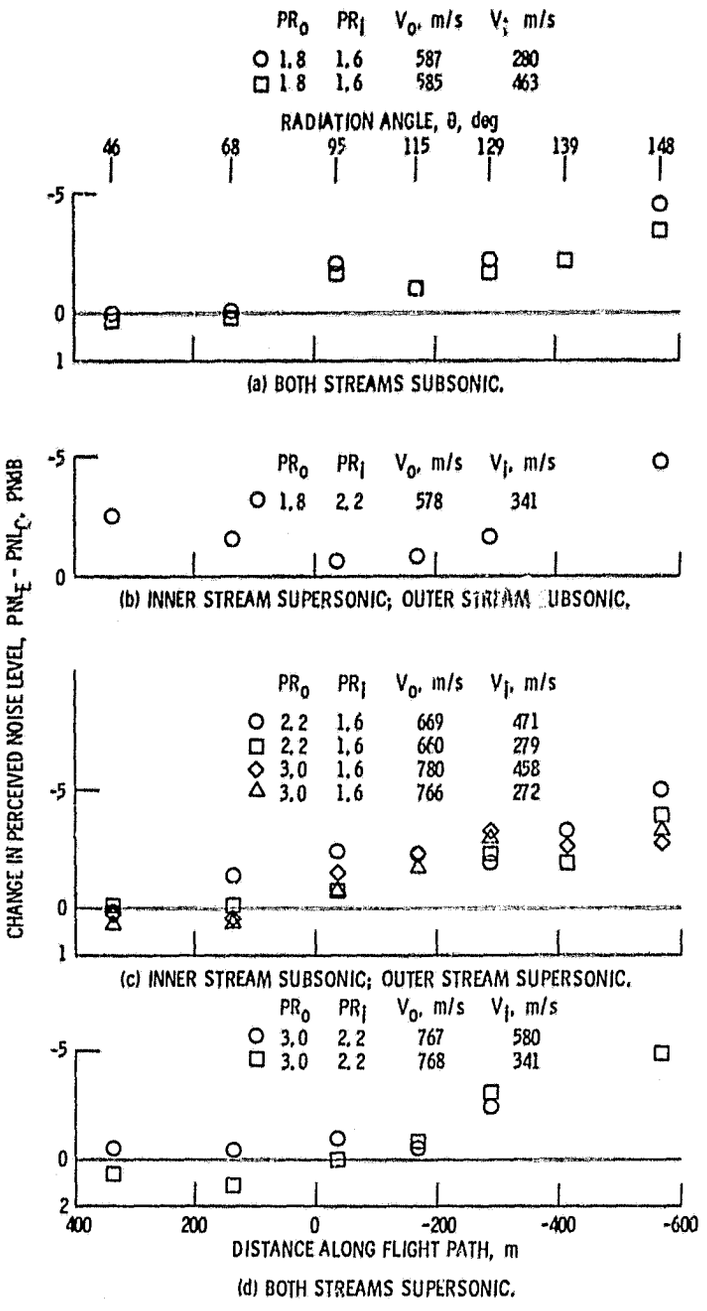

Figure 20. - Variation of PNL differences between concentric and eccentric nozzles as function of flyover distance.

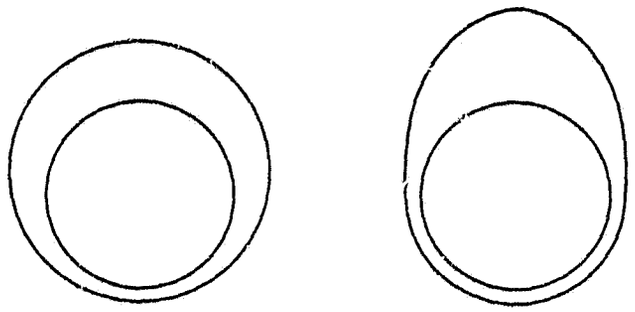

(a) PRESENT ECCENTRIC NOZZLE.

(b) PROPOSED ASYMMETRIC SHAPED NOZZLE.

Figure 21. - Annulus shaping for improved sideline noise suppression benefits.

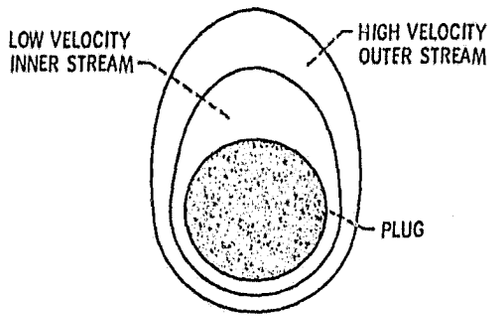

Figure 22. - Schematic of a possible dual stream IVP plug shaped-nozzle concept.